

# Cosmogenic nuclides, topography, and the spatial variation of soil depth

Arjun M. Heimsath <sup>a,\*</sup>, William E. Dietrich <sup>a</sup>, Kunihiro Nishiizumi <sup>b</sup>,  
Robert C. Finkel <sup>c</sup>

<sup>a</sup> *Department of Geology and Geophysics, University of California, Berkeley, CA 94720-4767, USA*

<sup>b</sup> *Space Sciences Lab, University of California, Berkeley, CA 94720, USA*

<sup>c</sup> *Center for Accelerator Mass Spectrometry, Lawrence Livermore National Laboratory, Livermore, CA 94550, USA*

Received 7 November 1997; revised 18 March 1998; accepted 14 May 1998

---

## Abstract

If the rate of bedrock conversion to a mobile layer of soil depends on the local thickness of soil, then hillslopes on uniform bedrock in a landscape approaching dynamic equilibrium should be mantled by a uniform thickness of soil. Conversely, if the depth of soil varies across an actively eroding landscape, then rates of soil production will also vary and, consequently the landscape will not be in morphologic equilibrium. The slow evolution of hillslopes relative to the tempo of climatic variations and tectonic adjustments would suggest that local morphologic disequilibrium may be expected in many landscapes. Here, we explore this issue of equilibrium landscapes through a previously developed model that predicts the spatial variation in thickness of soil as a consequence of the local balance between soil production and erosion. First, we confirm the assumption in the model that soil production varies inversely with the thickness of soil using two independent methods. One method uses the theoretical prediction that at local steady state (soil production equals removal), the depth of soil should vary inversely with hillslope curvature. The second method relies on direct measurements of in situ produced concentrations of cosmogenic <sup>10</sup>Be and <sup>26</sup>Al in bedrock at the base of the soil column. For our study site in Northern California, the two methods agree and yield the expression that the rate of soil production declines exponentially with the thickness of soil from 0.077 mm/year with no soil mantle to 0.0077 mm/year under 1 m of soil. We then use this function of soil production in a coupled production and diffusive model of sediment transport to explore the controls on the spatial variation of the depth of soil on four separate spur ridges (noses) where we measured the data for the function of soil production. Model predictions are sensitive to boundary conditions, grid scale, and run time. Nonetheless, we found good agreement between predicted and observed depths of soil as long as we used the observed function of soil production. The four noses each have spatially varying curvature and, consequently, have varying depths of soil, implying morphologic disequilibrium. We suggest that our study site has been subjected to a wave of incision and varying intensities of erosion because of tectonic and climatic oscillations that have a frequency shorter than the morphologic response time of the landscape. © 1999 Elsevier Science B.V. All rights reserved.

*Keywords:* geomorphology; cosmogenic nuclides; soil production; erosion; landscape evolution

---

\* Corresponding author. Fax: +1-510/643-9980; E-mail: arjun@geomorph.berkeley.edu

## 1. Introduction

Soil on hilly and mountainous landscapes is produced from underlying bedrock by various mechanisms and is transported downslope primarily by the processes of mass wasting and overland flow. Even predominantly soil mantled landscapes are rarely blanketed uniformly with soil. Instead, bedrock often crops out in locally steep areas, soils are typically thin to absent on narrow ridge crests, and soil tends to accumulate to considerable depths in valleys (e.g., Young, 1963; Arnett, 1971; DeRose et al., 1991; Dietrich et al., 1995; Gessler et al., 1995). This spatial variation in the thickness of soil may hold important clues about the pace and relative uniformity of landscape evolution.

Gilbert (1877) (pp. 103–105) suggested that the rate of conversion of bedrock to a mobile surface layer (soil) is a function of the overlying thickness of the soil mantle. If this is the case, then the simple observation that the thickness of soil varies across a landscape indicates that the rate of bedrock conversion to soil varies. This implies that different rates of lowering occur across the landscape and that the landscape is not in what Gilbert and then Hack (1960) called dynamic equilibrium. It is possible, however, that this is not the case. Ahnert (1987) demonstrated that spatial variation in the thickness of soil could occur if the relationship between the rate of soil production and the thickness of soil were to vary spatially across the landscape. This condition, perhaps because of variations in the underlying bedrock, would result in thin soils forming on rock more resistant to soil production and thick soils developing on rock more readily converted to soil. Such a state could result in identical rates of lowering and a hillslope with constant topographic curvature. Hack (1960) implied such a trade off between soil production and depth when he contrasted the slope morphology of quartzite versus shale in the Appalachians.

The suggestion that the local thickness of soil affects the rate of bedrock conversion to soil, and hence the rate of supply of erodable debris, has developed into a central theme in geomorphology, thanks largely to the clarity with which Carson and Kirkby (1972) wrote about the topic in their seminal book. They illustrated the Gilbert idea with a simple

cartoon of a function of soil production and suggested that landscapes tend to be in either a weathering-limited condition (where the potential erosion is greater than the production of soil and the land strips to bedrock) or a supply-limited state (where rates of erosion do not exceed rates of potential soil production). In more recent numerical modeling of landscapes, this theme has been highlighted (e.g., Anderson and Humphrey, 1989) as central to understanding the pace and form of landscape evolution. Tucker and Slingerland (1994), for example, conclude that the persistence of distinct passive margin rift topography, such as the Great Dividing Range of Australia, owes its origin to the emergence of a weathering limited condition preventing the rapid spread of erosion across the landscape.

Despite the central importance of the function of soil production to understanding landscape evolution (e.g., Rosenbloom and Anderson, 1994), little is known about it. As Cox (1980) described, two basic hypotheses exist about the probable shape of the function of soil production. The simplest hypothesis suggests that soil production is greatest when bedrock is just exposed, decreases with increasing depth of soil, and assumes that this decline is exponential. This was assumed to emulate the decreasing effectiveness of mechanical processes, such as freeze-thaw (Ahnert, 1967) or biogenic disturbance (Dietrich et al., 1995).

A more complicated function, first reasoned by Gilbert (1877, pp. 103–105) for frost and solution processes, suggested that rates of soil production are greatest under some finite depth of soil, decline with depths greater than the optimum, and are also lower than the optimum under shallower soils and exposed bedrock. This ‘humped’ function supports the intuition that some limiting depth of soil is required for animal burrowing or vegetative rooting, as well as the fact that water rapidly moves off bare bedrock. As soil thickens beyond the optimal depth, rates of soil production would decline similar to the inverse exponential function. As Carson and Kirkby (1972) and Dietrich et al. (1995) point out, however, an unstable positive feedback exists for soils thinner than the optimal depth. Changes in rates of erosion would either cause the soil to thicken to a stable depth, equal to or greater than the depth at the optimum, or strip the hillside to bedrock. The result

dictated by this model is that no equilibrium occurs in soil depths less than the optimal depth.

Here we present two independent methods that can be used to define quantitatively the function of soil production. We expand upon our initial findings on this topic (Heimsath et al., 1997) by using the documented function of soil production in a numerical model developed by Dietrich et al. (1995) to predict the local spatial variation of the depth of soil on individual convex ridges (called noses here) in our field area. The results of this modeling add strong support to the production function as well as the utility of the numerical model.

## 2. Theoretical framework

Our conceptual framework, using conservation of mass for a column of soil, to investigate the function of soil production is illustrated in Fig. 1. Commonly, the boundary between the soil mantle and the underlying weathered or fresh bedrock is abrupt and can be defined locally within a few centimeters ( $e$  in Fig. 1b). This boundary is not generally a chemical-weathering front associated with infiltrating water. Instead, it is a boundary that is defined by the mechanical disruptions of the underlying bedrock. Whereas wetting and drying, freeze-thaw, and similar processes can contribute to the advancing of this boundary into the rock, in many environments biogenic activity plays an important role in the mechanical disruption of the rock (e.g., Gilbert, 1877; Lutz,

1960; Johnson, 1990; and numerous other papers). The penetration of roots, tree throw, burrowing macrofauna (e.g., gophers and mountain beavers) and insects into the underlying rock are likely to be the main mechanisms of soil production in these environments (note gopher burrows in the saprolite,

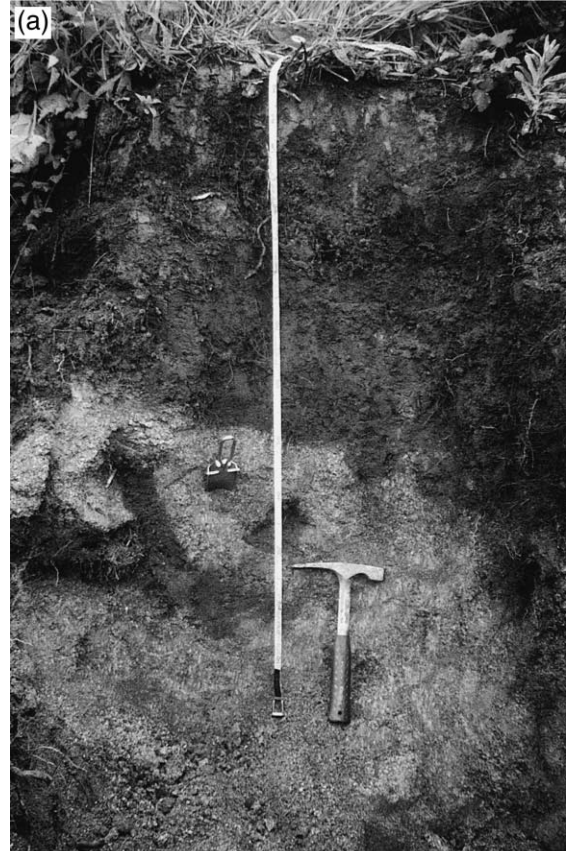


Fig. 1. (a) The conservation of mass equation for soil depth,  $h$ , states that the change in soil mass with time,  $t$ , is equal to the conversion of bedrock to soil because of lowering of the bedrock–soil interface less the divergence of transported soil mass. The area shown between the base of the soil at elevation,  $e$ , and the dashed line is the amount of bedrock that would be converted to soil over some specified time interval. In this study area, mass transport,  $\tilde{q}_s$ , of the entire active layer of soil is caused primarily by biogenic processes acting on an inclined surface. Note that  $z = e + h$ , a bedrock-fixed coordinate system not accounting for tectonic influences on absolute elevation, and  $h \ll$  the scale of landscape elevation set by the total relief. (Modified from Dietrich et al., 1995). (b) Photograph of a typical soil-weathered bedrock boundary with gopher burrow shown penetrating the saprolite. Soil depth,  $h$ , is 60 cm.

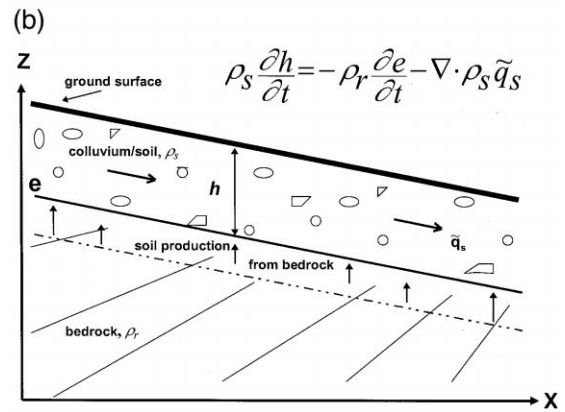


Fig. 1b). Soil horization is typically limited in such regions and, therefore, such soils have received relatively little attention by pedologists.

We write the mass conservation equation for the depth of soil,  $h$ , to represent the balance between the local rate of soil production,  $-(\partial e)/(\partial t)$ , and the divergence of the sediment transport vector,  $\tilde{q}_s$ , as,

$$\rho_s \frac{\partial h}{\partial t} = -\rho_r \frac{\partial e}{\partial t} - \rho_s \nabla \cdot \tilde{q}_s \quad (1)$$

where  $\rho_s$  and  $\rho_r$  are the bulk densities of soil and rock, respectively, and  $e$  is the elevation of the bedrock–soil interface in a bedrock-fixed coordinate system. Dissolution is not specifically modeled. Instead, we account for dissolution effects by measuring the bulk densities of samples taken from the field. The intensity of chemical weathering of the bedrock undoubtedly affects the local rate of soil production. This effect is treated empirically as part of the function of soil production.

The simplest law for the transport of hillslope sediment was first articulated by Davis (1892) and Gilbert (1909) and states that sediment flux,  $\tilde{q}_s$ , is proportional to slope,  $\nabla z$ , such that,

$$\tilde{q}_s = -K \nabla z \quad (2)$$

where  $K$  is equivalent to a diffusion coefficient with units of  $L^2/t$  and  $z$  is the elevation of the ground surface. This diffusive transport law is most appropriately applied to hillslopes where no erosion occurs by overland flow and shallow landsliding is rare or absent. Some field evidence exists to support the linear dependency of sediment flux on slope (McKean et al., 1993), and the diffusivity,  $K$ , can be estimated with various field measurements (e.g., Fernandes and Dietrich, 1997). Diffusive sediment

transport is widely assumed and is used in extensive applications of analytical and numerical models of landscape evolution (Culling, 1963; Kirkby, 1971; Armstrong, 1987; Anderson and Humphrey, 1989; Koons, 1989; Howard, 1994, 1997; Kooi and Beaumont, 1994; Tucker and Slingerland, 1994; also see Ellis and Merritts, 1994). Dietrich et al. (1995) and Reneau and Dietrich (1991) use it to represent biogenic transport and McKean et al. (1993) found it applicable to soil creep.

We substitute this transport law into Eq. (1) and solve for soil production:

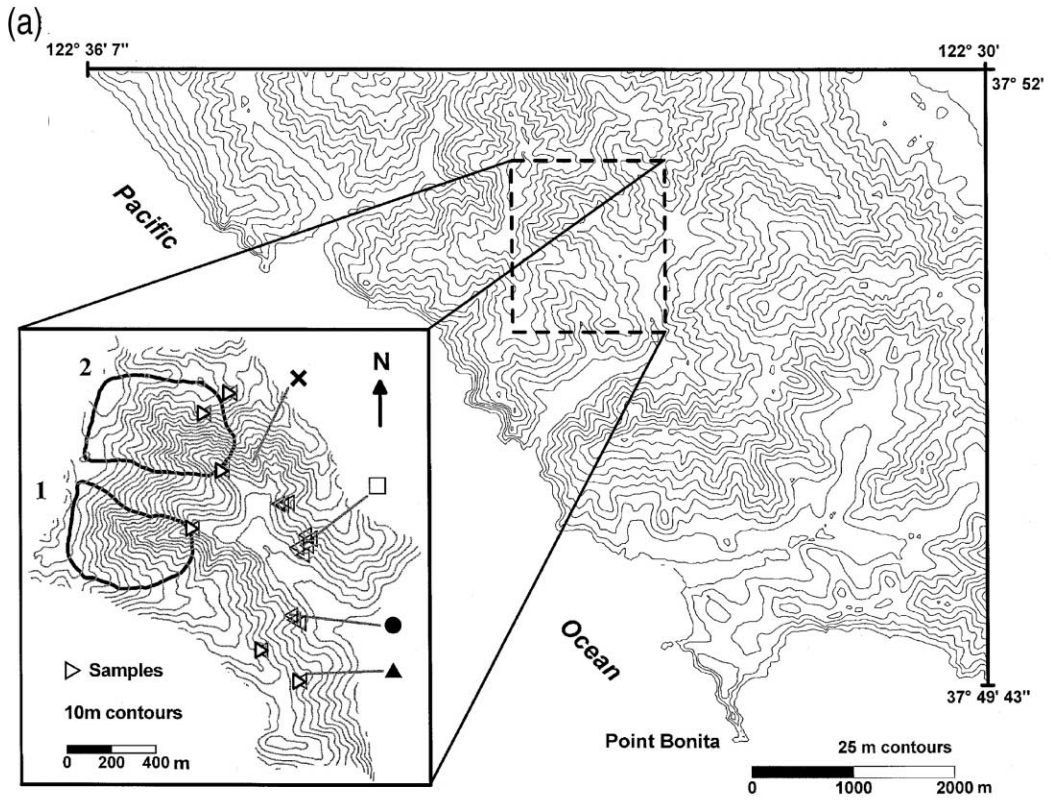
$$\frac{\partial e}{\partial t} = -\frac{\rho_s}{\rho_r} \frac{\partial h}{\partial t} - \frac{\rho_s}{\rho_r} K \nabla^2 z \quad (3)$$

If the local depth of soil does not vary significantly over time (i.e.,  $dh/dt = 0$ ) then steady state conditions apply, where soil production is balanced by soil removal, and:

$$\frac{\partial e}{\partial t} = -\frac{\rho_s}{\rho_r} K \nabla^2 z \quad (4)$$

Eq. (4) states that if the local depth of soil is constant over time, then soil production is proportional to the negative of the topographic curvature,  $-\nabla^2 z$  (i.e., topographic divergence is negative with units of  $L^{-1}$  and, therefore, positive soil production occurs on divergent parts of the landscape while soil accumulates in the convergent regions). In convergent areas,  $dh/dt \neq 0$  because of accumulation and Eq. (4) does not apply. The assumption of local steady-state depth of soil is central to both our methods, hence, our investigation focuses on divergent areas (ridges) where linear diffusive sediment transport processes are likely to be predominant.

Fig. 2. (a) Site location for Tennessee Valley, Marin County, CA. Regional topography is shown from part of the Point Bonita, CA USGS 7.5 min quadrangle with 25 m contour lines. The Golden Gate Bridge is directly east of the scale bar. The inset map is this field area shown with 10 m contour lines drawn from high resolution digital data (modified from Heimsath et al., 1997). Open triangles on the inset map show sample locations for the cosmogenic nuclide samples. Large bedrock outcrops were sampled from the upper region in sub-basin 2 as well as from a ridge top near two of the surveyed noses. Nose surveys are located with the symbols ( $\times$ , open square, black circle, and black triangle) and correspond to the upper-corner symbols on the individual maps of Figs. 5 and 9. The two nuclide samples at the base of sub-basins 1 and 2 are stream sediment samples. (b) Photograph of Tennessee Valley with sub-basins 1 and 2 labeled, large bedrock outcrop, TV-4 shown, and surveyed noses numbered corresponding to Figs. 5 and 9.



### 3. Field site

The location of our field area in Tennessee Valley, Marin County, California is shown on part of the Point Bonita 7.5 min USGS topographic map (USGS DEM) (Fig. 2a,b). Extensive geomorphic research has been conducted in this area and on nearby regions (e.g., Reneau et al., 1986, 1990; Montgomery and Dietrich, 1988, 1989, 1995; Black and Montgomery, 1991; Dietrich et al., 1992, 1993, 1995). Intensely sheared thrust sheets of greenstone, greywacke sandstone and chert, typical of the Jurassic–Cretaceous Franciscan assemblage in the Marin Headlands terrane underlie the field area (Wahrhaftig, 1984). The area receives an average annual rainfall of 760 mm (Rantz, 1968) and was grazed prior to 1972. There is no evidence that Quaternary climatic variation caused dramatic changes in the processes of hillslope erosion. Net sediment storage in valleys and landslide frequency in unchanneled valleys (hollows) may have varied, however, because of changes in the intensity of the erosional processes (Reneau et al., 1986, 1990; Rypins et al., 1989). While partial forest cover existed in the Pleistocene, no evidence occurs for a Holocene forest. The vegetation is a mixture of coastal grassland and scrub (coyote brush (*Baccharis pilularis*), poison oak (*Rhus diversiloba*), and many introduced herbaceous species and grass). In colluvium mantled hollows, exfiltrating water and rain develop extended areas of saturation overland flow (Dietrich et al., 1993, Montgomery and Dietrich, 1995). The soil mantle varies in thickness across the landscape and on the ridges is typically an organic-rich, stony loam with weak to no horizonation. Soil production is likely to result primarily from the mechanical disruption of weathered bedrock by biogenic activity (Dietrich et al., 1995). Soil and rock fragments from pocket gopher (*Thomomys bottae*) burrows litter the ground surface, and soil pits show clear evidence of burrows intersecting the typically abrupt transition to the underlying saprolite or weathered bedrock (Fig. 1b). Burrowing is also the primary mechanism for downslope soil transport (Black and Montgomery, 1991) and effective diffusivities for this biogenic transport have been quantified based on rates of infilling in hollows (Reneau et al., 1986, 1990; McKean et al., 1993; Dietrich et al., 1995). Landsliding is mostly

confined to steep hollows where thick colluvial deposits have accumulated (Dietrich et al., 1992; Dietrich et al., 1993).

### 4. Soil depth and curvature

#### 4.1. Method

We relate the rate of soil production to the depth of soil to quantify the function of soil production by using two distinct methods. Our first method applies Eq. (4) to noses where processes of diffusive sediment transport are assumed to be dominant. On convex regions of the landscape, local soil production is equal to local topographic curvature multiplied by a constant. The form of the function of soil production, that is,

$$-\frac{\partial e}{\partial t} = f(h), \quad \text{where} \quad f(h) = -\frac{\rho_s}{\rho_r} K \nabla^2 z \quad (5)$$

can, therefore, be determined by field measurements of topographic curvature plotted against measurements of the depth of soil from the same location. The depth of soil is measured to the base of the soil column (Fig. 1). Soil pits were dug perpendicular to the local slope and usually extended beyond the obvious soil–bedrock boundary to insure proper identification of the boundary. Because of uncertainty with the auger measurements, we relied primarily on pits for the measurements of soil depth. If the diffusivity,  $K$ , is known and the bulk densities of soil and rock are measured, then the function of soil production can be fully quantified for the field site.

We have experimented with several different algorithms to calculate curvature,  $\nabla^2 z$ , on a landscape. All calculations use high-resolution elevation data from total station surveys, although elevation data obtained by any method can be used in the same process. For all but one of the methods (which used the raw survey data and is mentioned below), the calculations of curvature used data gridded from survey points by *Kriging* (Cressie, 1991) using SURFER<sup>®</sup> software. Other interpolation schemes be-

sides *Kriging* (e.g., minimum curvature, inverse distance to a power, nearest neighbor, polynomial regression, and triangulation with linear interpolation) resulted in grid artifacts that misrepresented, or even completely transformed, the real topography.

We calculate curvature at a point using the eight nearest neighbors (e.g., Moore et al., 1993a,b) with an algorithm similar to the one used by Dietrich et al. (1995). To illustrate our method, we focus on a small, representative piece of a convex nose from one of our field surveys (Fig. 3).  $\nabla^2 z$  at the central grid node, #5 posted above the +, is calculated with the elevations,  $E_n$ , of the nearest eight grid nodes,

$$\nabla^2 z = \frac{2(E_2 + E_4 + E_6 + E_8) + (E_1 + E_3 + E_7 + E_9) - 12E_5}{4b^2} \quad (6)$$

The subscript numbers correspond to the numbers posted above the symbols of the grid nodes and  $b$  is the width of the cell.  $\nabla^2 z$  is calculated with Eq. (6) for every grid node on the landscape and is interpolated to yield curvature at the depth-sample locations, shown for example by the black dot above node #5.

A similar algorithm for calculating curvature uses the elevations of the nearest points of the topographic survey (the small dots in Fig. 3). Such use of real data rather than interpolated data is computationally more involved and involves moving a fixed-size window (equivalent conceptually to choosing a grid scale) to every measurement of depth and using all survey measurements within that window to calculate curvature. Because little difference exists in the calculated  $\nabla^2 z$  between the methods we chose the grid-based algorithm for its computational simplicity and applicability to any grid-based landscape model (see Moore et al., 1991 for discussion of digital data sources). The data from the grid yield a best-fit surface to the local points. Because we are most interested in the trend of the topography, not in the centimeter scale heterogeneity captured by placing the survey rod on small bumps or troughs on the ground surface this best-fit surface seems appropriate. Very good agreement exists between the grid for topography and the real survey points, with no obvious grid artifacts.

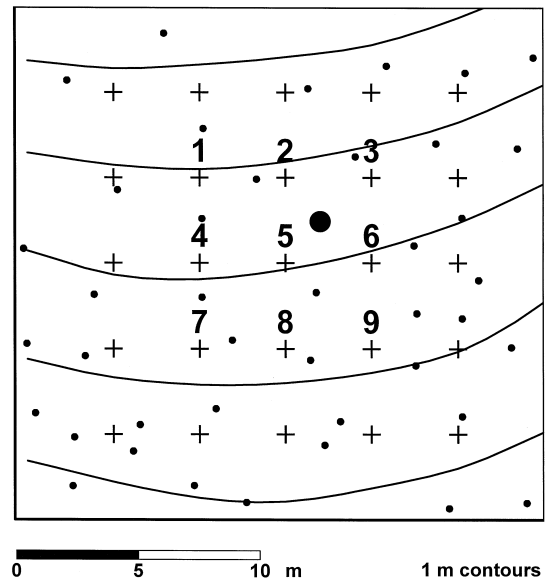


Fig. 3. A representative area from a surveyed nose. Grid node locations from a 3.5-m grid interpolated from the original survey data are shown by '+'s. Locations of survey points are shown by the small dots for this area. The large dot above grid-node 5 shows the location of one measurement of soil-pit depth. Contour lines are drawn at 1 m intervals. Curvature at every node is calculated using Eq. (6) in the text, written to illustrate the curvature calculation for grid-node 5. Curvature calculated in this manner is then interpolated from all adjacent grid nodes to determine the curvature at the location of the depth measurement.

One complicating factor in finding a robust method for calculating curvature is determining the appropriate scale of the topographic grid. We surveyed our field areas at very high resolutions to allow us to explore the effects of various sizes of grids (ranging from 1.5 m to 20 m) on calculated curvature. Fig. 4 shows an example of the effect of size of grid on curvature. For this example, curvature is plotted as a function of grid size for 21 points of depth on one of the surveyed noses. The curvature becomes relatively scale-independent at grid scales greater than 5 m. We applied such an analysis to all the measurements of depth for this study and determined that a 5 m grid size was the finest size above which curvature was not sensitive to the scale of the grid. Grids with higher resolutions produce large local variances in curvature as the micro-topography approaches the scale of gopher mounds and animal trails. Conversely, sizes of grids greater than about

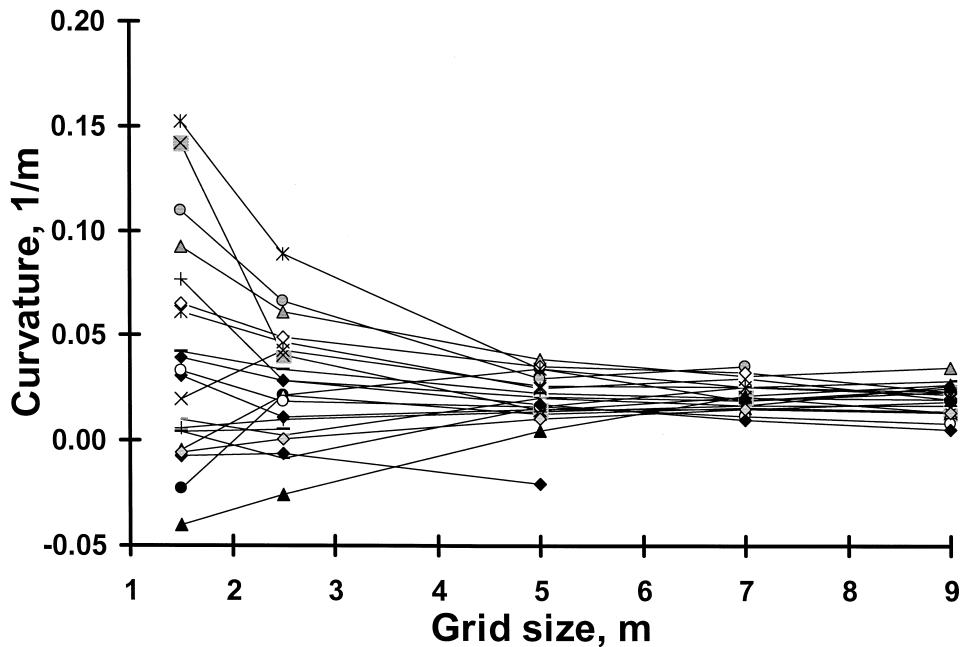


Fig. 4. An example of how grid size effects the calculated curvature for 21 measurements of depth from one of the noses shown in Fig. 5. Categories of grid sizes are 1.5, 2.5, 5, 7, and 9 m. Curvature becomes scale-independent at the 5 m grid size. We applied this method with grid sizes up to 20 m for all four of our surveyed noses shown in Fig. 5 with all measurements of depth and found that, in general, 5 m was the grid size that best characterized the land surface. Depth measurements with negative curvatures (concavity), or strongly scale dependent curvatures were not used for determining the function of soil production.

10 m tend to smooth the landscape beyond the scale of the biota affecting the depth of soil in this field area (i.e., no large trees exist). The optimal scale of the grid is likely to be different for landscapes under different dominant processes or climates.

#### 4.2. Results

Four convex noses surveyed for this analysis are located in the study catchment by the symbols on the inset map of Fig. 2. These noses were chosen for the relatively high degree of curvature and for relatively gentle ( $< 25^\circ$ ) slopes to avoid the possible influence of shallow landsliding. All four noses were surveyed with a total survey station at a 1–3 m resolution. Each nose is primarily underlain by greywacke sandstone, although noses 2 and 4 had prominent outcrops of greenstone near the areas surveyed for this study. Fig. 5 illustrates the topography of these noses

with 2 m contour intervals. We intentionally surveyed divergent regions away from potential boundary affects such as the ridge crests and deep colluvial fills in the convergent hollows.

An inverse relationship exists between curvature and the depth of soil on these noses (Fig. 6) which, if curvature is a surrogate for the production of soil, defines the form of the function of soil production. The symbols plotted on Fig. 6 correspond to the upper-corner symbol on each topographic map and suggest that each individual nose may define a slightly different relationship between soil production and depth. If this is indeed the case, and a single function of soil production exists for the underlying greywacke, then different noses may be producing soil, and, therefore, lowering at different rates.

The variance in this curvature–depth relationship can be explained in two ways. The production of soil by biota may be thought of as stochastic processes acting on a landscape and causing significant short-

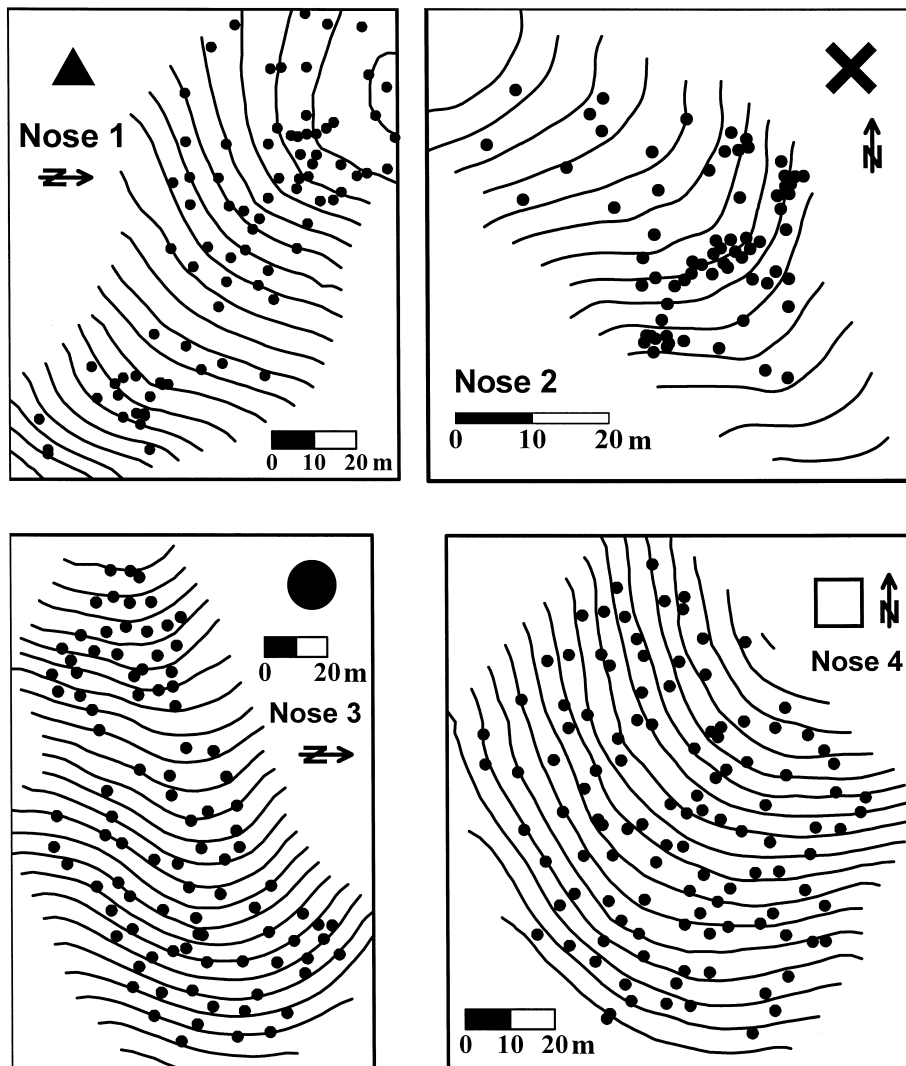


Fig. 5. The four noses surveyed for our curvature analyses are located on Fig. 3 inset map with the upper-corner symbols. We surveyed the topography at about 1–3 m resolutions and the 2 m contour lines shown here are drawn from 3.5 m grids generated by a *Kriging* interpolation scheme. Dots on the noses show locations of the depth measurements from either auger holes or pits and are equivalent to the large dot on Fig. 3.

term variations in the local depth of soil (e.g., Johnson, 1990). For example, animal burrowing can create local mounds of soil that will be ‘smoothed’ away by downslope sediment transport. Where this burrowing causes mechanical disruption of the bedrock, the soil will thicken locally. Hence, local variations in the depth of soil for a given curvature are created by the surface variations associated with

pit and mound topography and by the subsurface variations in the bedrock surface because of local disturbances. The other source of variability in the depth of soil is bedrock heterogeneity, which leads to a variance in resistance to weathering and mechanical disruption by biota. This can lead to a similar curvature and rate of erosion under different depths (Ahnert, 1987). Despite these sources of variance,

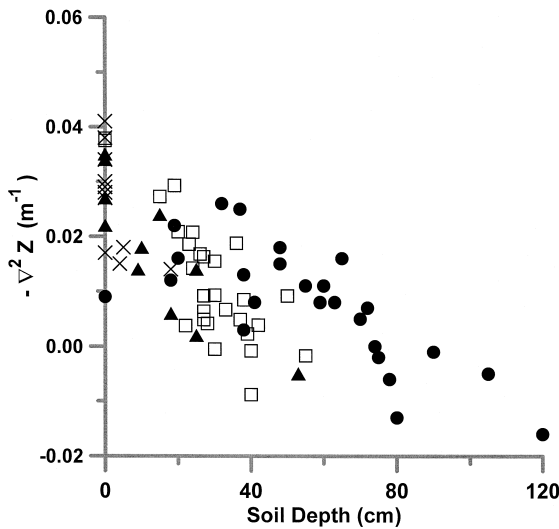


Fig. 6. Negative hillslope curvature (divergent slopes are positive),  $-\nabla^2 z$ , in  $\text{m}^{-1}$ , against measured local depth of soil, in cm, from the noses shown in Fig. 5. The symbols correspond to the upper-corner symbols on the individual noses. Curvature was calculated by the method illustrated in Fig. 3 and Eq. (6) in the text. Data plotted here retained the same curvature over the grid sizes and eliminate some of the points plotted on the maps because of insufficient survey points. We plot deeper depths here despite the weak concavities to show the strong inverse trend of the data over the range of the depths measured on Nose 3. (Modified from Heimsath et al., 1997.)

we interpret our observations of curvature and depth as showing a central tendency for thickness to increase with decreasing curvature.

## 5. Cosmogenic nuclides and soil depth

### 5.1. Method

As an independent test of the function of soil production determined from morphometry we use concentrations of cosmogenic nuclides in bedrock to infer long-term rates of erosion (see reviews in Lal, 1991; Nishiizumi et al., 1993; Bierman, 1994; Cerling and Craig, 1994). Our method relies upon measuring the concentrations of in situ produced cosmogenic  $^{10}\text{Be}$  ( $t_{1/2} = 1.5 \times 10^6$  y) and  $^{26}\text{Al}$  ( $t_{1/2} = 7.01 \times 10^5$  y) extracted from the target mineral quartz in bedrock (Lal and Arnold, 1985; Nishiizumi

et al., 1986; Lal, 1988; Lal, 1991; Nishiizumi et al., 1991). If we assume that the conversion of bedrock to soil reaches a steady state under a constant depth of soil,  $h$ , (and the soil bulk density remains constant) then, the concentration of the cosmogenic radionuclide,  $C$  (atom/g), in the bedrock at the soil-bedrock interface is,

$$C = P(h, \theta) \left( \frac{1}{\lambda + \frac{\rho_t \varepsilon}{\Lambda}} \right) \quad (7)$$

where  $P(h, \theta)$  is the rate of production of the nuclide (atom/y) at depth  $h$  and slope  $\theta$ ,  $\Lambda$  is the mean length of attenuation ( $\sim 165$  g/cm<sup>2</sup>),  $\lambda$  is the decay constant of the radionuclide and ( $\lambda = \ln 2/t_{1/2}$ ) and  $\varepsilon$  is the rate of conversion of bedrock to soil (cm/y) (i.e.,  $-\partial e/\partial t$  in Eq. (1)). Eq. (7) is of the same form as that used by others to calculate the rate of erosion of bedrock (in which case,  $h$  and  $\theta = 0$ ) (Lal and Arnold, 1985; Nishiizumi et al., 1991). We can rearrange Eq. (7) to solve for the conversion rate of rock to soil as a function of either measurable or known quantities such that,

$$\varepsilon = -\frac{\partial e}{\partial t} = \frac{\Lambda}{\rho_t} \left( \frac{P(h, \theta)}{C - \lambda} \right) \quad (8)$$

The rates of production of  $^{10}\text{Be}$  and  $^{26}\text{Al}$  in quartz are known at the ground surface as functions of latitude, elevation and topographic shielding (Lal, 1991; Nishiizumi et al., 1989). We measured the bulk density and depth of soil individually. Most of our samples are taken from hillsides with slopes between 10 and 30°, which effects the relative exposure to cosmic ray flux. Nishiizumi et al. (1989) discuss the implications of sampling from inclined surfaces, referring to the original observation of Lal (1958) that the angular distribution of cosmic ray particles in the troposphere is given by  $F(\theta) = \sin^2.3\theta$ . This simple correction for slope is combined with a depth correction (Nishiizumi et al., 1991, Eq. (1)) for the rate of production of nuclides when the bedrock sample is under a depth of soil and the soil mass shields the bedrock from the penetration of cosmic rays (Lal, pers. comm. 1996). We use the soil

bulk density and assumed steady-state soil depths (Table 1) to calculate the shielding mass used for the depth correction.

We sampled bedrock in soil pits from the continuous layer of rock at the soil–bedrock boundary and from exposed bedrock (the  $h = 0$  samples). Sampling pits extended below this boundary to insure accurate local measurement of the boundary. We excavated the top 1–3 cm of bedrock from the in-place bedrock with a chisel and hammer. About 1–3 kg of bedrock were required to insure 40–60 g of quartz remained after rock crushing and chemical separations. Chemical separation and purification of quartz from the sampled rock followed the procedure outlined by Kohl and Nishiizumi (1992). We used four 10-h ultrasonic leaches, however, compared to the normal three leaches that are typically sufficient for ‘cleaner’ quartz. This insured removal of any meteoric (garden variety)  $^{10}\text{Be}$  remaining in the sample and helped reduce the background concentration of  $^{27}\text{Al}$ . The quartz contained high levels of titanium, which can potentially scavenge Al from the analysis

solution by co-precipitation. Each precipitate was, therefore, treated at least twice with sulfuric acid. No significant residue ( $< 1$  mg) remained after this treatment and we found no evidence of scavenged Al. We measured background concentrations of  $^{27}\text{Al}$  by AA. We used a Be carrier calibrated by Nishiizumi’s Be AA standard and it differed by less than 2% from the Be carrier used for the Nishiizumi et al. (1989) analyses.

$^{10}\text{Be}$  and  $^{26}\text{Al}$  concentrations were measured at the LLNL-CAMS facility (Davis et al., 1990) and the measured ratios were normalized to the ICN  $^{10}\text{Be}$  and the NBS  $^{26}\text{Al}$  standards. Rates of soil production rates were calculated from these concentrations using Eq. (8) and the depth-slope correction factor for samples from under the full range of soil depths. We quantified the function of soil production by plotting these rates against the measured depth of soil. As a separate measure of the average rates of soil erosion from the hillsides, we sampled stream sediments from sub-catchment outlets (Bierman and Steig, 1996; Granger et al., 1996). We also sampled three

Table 1  
Measurements of cosmogenic nuclide concentrations

Sample	Depth (cm)	Slope (deg)	Elevation (m)	Quartz wt. (g)	$^{26}\text{Al}$ ( $10^6$ atom/g)	$^{10}\text{Be}$ ( $10^6$ atom/g)	$^{26}\text{Al}/^{10}\text{Be}$	$h$ -slope factor	$-de/dt$ (m/My)
TV-2	0	8	135	40.65	$0.600 \pm 0.101$	$0.115 \pm 0.006$	$5.22 \pm 0.92$	1	$39 \pm 8$
TV-3	16	10	120	40.06	$0.447 \pm 0.054$	$0.108 \pm 0.007$	$4.15 \pm 0.56$	0.87	$47 \pm 15$
TV-4	0	15	275	42.68	$1.132 \pm 0.078$	$0.248 \pm 0.010$	$4.55 \pm 0.37$	0.98	$20 \pm 5$
TV-5	0	0	275	40.22	$1.433 \pm 0.121$	$0.351 \pm 0.017$	$4.08 \pm 0.40$	1.00	$15 \pm 4$
TV-6	35	15	105	42.03	$1.104 \pm 0.050$	$0.195 \pm 0.008$	$5.65 \pm 0.34$	0.69	$26 \pm 3$
TV-7	58	20	100	42.58	$1.446 \pm 0.061$	$0.229 \pm 0.016$	$6.32 \pm 0.52$	0.52	$21 \pm 3$
TV-10	51	17	115	40.71	$0.939 \pm 0.104$	$0.171 \pm 0.011$	$5.49 \pm 0.71$	0.59	$25 \pm 4$
TV-11	0	21	120	32.39	$0.234 \pm 0.035$	$0.040 \pm 0.005$	$5.85 \pm 1.20$	0.98	$107 \pm 23$
TV-12	30	15	116	40.56	$0.394 \pm 0.091$	$0.074 \pm 0.006$	$5.28 \pm 1.30$	0.72	$60 \pm 16$
TV-13	49	18	140	40.03	$1.060 \pm 0.112$	$0.151 \pm 0.013$	$7.03 \pm 0.95$	0.61	$26 \pm 5$
TV-15	20	15	135	40.33	$0.563 \pm 0.055$	$0.083 \pm 0.006$	$6.77 \pm 0.83$	0.85	$48 \pm 8$
TV-16	35	20	133	45.05	$0.741 \pm 0.076$	$0.134 \pm 0.007$	$5.54 \pm 0.64$	0.68	$33 \pm 5$
TV-17	60	25	133	52.57	$0.914 \pm 0.093$	$0.161 \pm 0.015$	$5.68 \pm 0.77$	0.54	$27 \pm 5$
TV-23	0	15	137	40.28	$0.260 \pm 0.051$	$0.050 \pm 0.005$	$5.16 \pm 1.14$	0.98	$91 \pm 24$
creek1a	n/a	n/a	110	51.50	$0.414 \pm 0.053$	$0.063 \pm 0.005$	$6.61 \pm 1.00$	1	$64 \pm 12$
creek1b	n/a	n/a	110	40.22	$0.366 \pm 0.050$	$0.063 \pm 0.006$	$5.81 \pm 0.95$	1	$66 \pm 13$
creek2	n/a	n/a	110	58.22	$0.239 \pm 0.049$	$0.041 \pm 0.005$	$5.87 \pm 1.37$	1	$102 \pm 25$

Concentration errors include  $1 \sigma$  from AMS.

All errors propagated to  $-de/dt$ .

Average soil density:  $1.4 \text{ g/cm}^3$

Location:  $37.9 \text{ N Lat.}, 122.6 \text{ W Long.}$

$^{26}\text{Al}$  and  $^{10}\text{Be}$  production rates are corrected for elevation and location (Lal, 1991; Nishiizumi et al., 1989).

$h$ -slope factor corrects for soil depth and slope shielding (Lal, pers. comm.).

isolated, large bedrock outcrops to determine the relative rates of erosion of such features in a predominantly soil mantled landscape.

## 5.2. Results

We determined the function of soil production from the cosmogenic nuclide-based method (Fig. 7). The rates of soil production were calculated from in situ produced  $^{10}\text{Be}$  and  $^{26}\text{Al}$  and averaged (Table 1). Each of the samples shown by the solid black circles were weathered greywacke bedrock with densities of  $2.2\text{ g/cm}^3$ . The variance-weighted least squares best

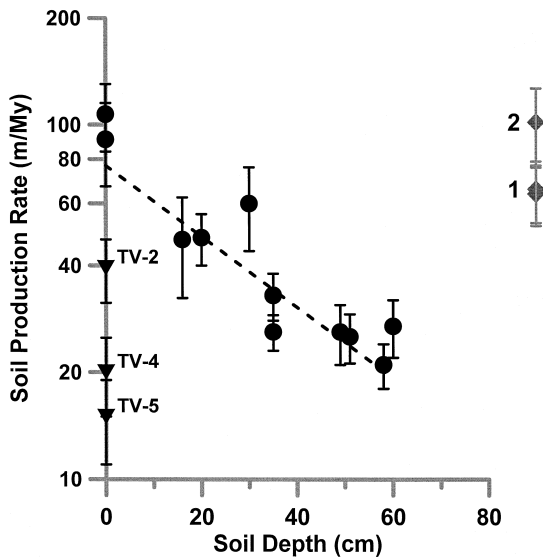


Fig. 7. Rates of soil production,  $-(\partial e)/(\partial t)$  in m/My, calculated from in situ produced cosmogenic  $^{10}\text{Be}$  and  $^{26}\text{Al}$  in bedrock samples versus measured depths of soil,  $h$ , in cm. We plot the rates calculated from concentrations of both nuclides (Table 1). The variance-weighted least squares best fit to these data is  $-(\partial e)/(\partial t) = (77 \pm 9)e^{(-0.023 \pm 0.003)h}$ . Upside down triangles show large, exposed bedrock samples with different lithologies and different locations from the samples used for the function of soil production. Both TV-4, a large,  $\sim 25\text{ m}$  relief, greenstone, and TV-5, a 3-m high bedded chert, were sampled from the top of basin 2 shown on the inset map of Fig. 2. TV-2 was from a large, coherent greywacke at the crest of the ridge above noses 1 and 3. The diamonds off the depth axis show basin-average rates of erosion from two samples of stream sediment taken from sub-basin 1 and one sample from sub-basin 2. Error bars are  $1\sigma$  propagated from AMS, AA, bulk density, absorption mean free path, and soil depth uncertainties. (Modified from Heimsath et al., 1997.)

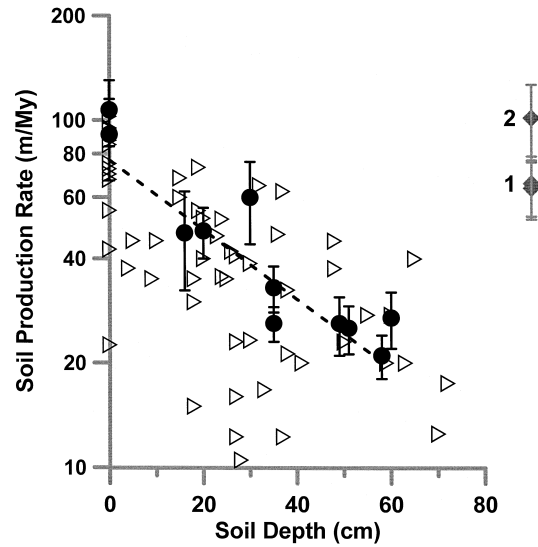


Fig. 8. The function of soil production from both of our independent methods. The curvature measurements from Fig. 6 are converted to rates of soil production using Eq. (4) in the text and are plotted as open triangles on the same axes as Fig. 7. We used a regional average diffusivity of  $50\text{ cm}^2/\text{y}$  (Reneau (1988), reported in McKean et al. (1993) and used in Dietrich et al. (1995)) and an average bulk density ratio of 0.5 without any attempt to adjust the parameters to improve the fit.

fit (Bevington, 1969) to these data shows an exponential decline of soil production with increasing depth of soil,

$$-\frac{\partial e}{\partial t} = (77 \pm 9)e^{(-0.023 \pm 0.003)h} \quad (9)$$

in which the units for the coefficient are m/My and the depth value,  $h$ , in the exponent is cm. The upside-down triangles show erosion rates of prominent, isolated bedrock outcrops. All are eroding at significantly slower rates than the exposed greywacke sampled from the surface of the soil-mantled landscape. Greywacke (TV-2) is eroding more rapidly than greenstone (TV-4, visible as the large outcrop at the head of the valley in Fig. 2a) and chert (TV-5). Sub-catchment samples are shown by the numbers 1 and 2 and show relatively high average rates of erosion for the respective outlined sub-basins on the Fig. 2a inset map.

To compare results from the two methods we converted our measured hillslope curvatures,  $-\nabla^2 z$

from Fig. 6, to rates of soil production according to Eq. (4) using an independently determined regional diffusivity of  $50 \text{ cm}^2/\text{y}$  (data from Reneau (1988), reported in McKean et al. (1993), and used in Dietrich et al. (1995)), and an average bulk density ratio of 0.5. Fig. 8 shows a direct overlay of these values of soil production on the nuclide-based results plotted in Fig. 7. We emphasize that no parameters were adjusted to compare these data from the two completely independent methods. The similarity between these two data sets supports considerably these two approaches. This suggests that we should be able to use Eq. (9) in a numerical model to predict the local soil depths.

## 6. Numerical modeling of soil thickness

### 6.1. Method

We used our function of soil production to predict the thickness of soil by adapting the model proposed by Dietrich et al. (1995). The model solves Eq. (1) by finite differences, adjusting soil production as a function of the local soil depth at each time step. The surface topography evolves such that after each time step the local flux and rates of soil production are recalculated. Here, Eq. (9) was used for the function of soil production and the model was applied to real topography from the four individual noses shown in Fig. 5. The model was run with 10-year time intervals using the smallest grid (1.5 m) that closely fit the survey data for the noses. Sediment is transported to and from the eight nearest grid cells as a function of gradient with a  $\sqrt{2}$  correction applied to the diagonals to account for the greater length of transport. If depth of soil thins to zero at a grid node, and downslope gradient demands more sediment than is available, then all sediment produced and received from above is transported out. We determined the total time that the model was run, in part, by plotting the predicted depths of soil against time and identifying the time at which the rate of soil depth increase declined significantly. This point was chosen to approximate the time when the local depth of soil had reached steady state and soil removal balanced soil production.

We needed to specify three boundary conditions to change the application of the model from the catchment scale (Dietrich et al., 1995) to the nose scale. At the upslope boundary of the noses, we set the maximum possible influx of sediment equal to the maximum rate of soil production of  $77 \text{ m/My}$ . This is equivalent to the weathering-limited condition of exposed rock such that the upper bound of the noses can only be supplied with sediment that is available from the single row of boundary grid cells. We chose this condition to represent the thin soil and exposed bedrock near the crests of noses 1 and 3 and the upper end of noses 2 and 4 (the upper boundaries of our surveyed regions). Boundaries along the sides of the surveyed noses were set to remove any sediment transported to them to avoid the accumulation of sediment. These side boundaries represent a condition of steady state elevation where an exact balance exists between inflow and outflow of sediment, and attempts to represent the position of the study areas (where depths were measured) well above the sediment accumulation zone of the hollows. The lowermost boundary is set to lower at a rate equal to the rate of soil production under the field-observed average depth of soil for the lower boundary of the respective nose. This condition maintains the observed landscape position of our surveyed noses above the sediment accumulation zone near the valley bottoms and, therefore, reduces flattening of the topography during the model runs. We specified zero depth of soil across each of the noses for our initial condition for the results reported here. As a means of comparison, we also ran the model with an initial depth of soil of 30 cm.

### 6.2. Results

The model predicts the thickness of soil to be thinnest on the nose axes and to be locally highly variable (Fig. 9). In general, thickness of soil increases downslope away from the nose crests. The very thin soils at the top of each nose are an artifact of the upslope boundary condition. We avoided this artifact in our comparison of observed with the predicted depths of soil by using only the observations below the highlighted contour lines of Fig. 9. Regions of thicker soils correspond to weakly divergent or slightly convergent areas on the noses. In a

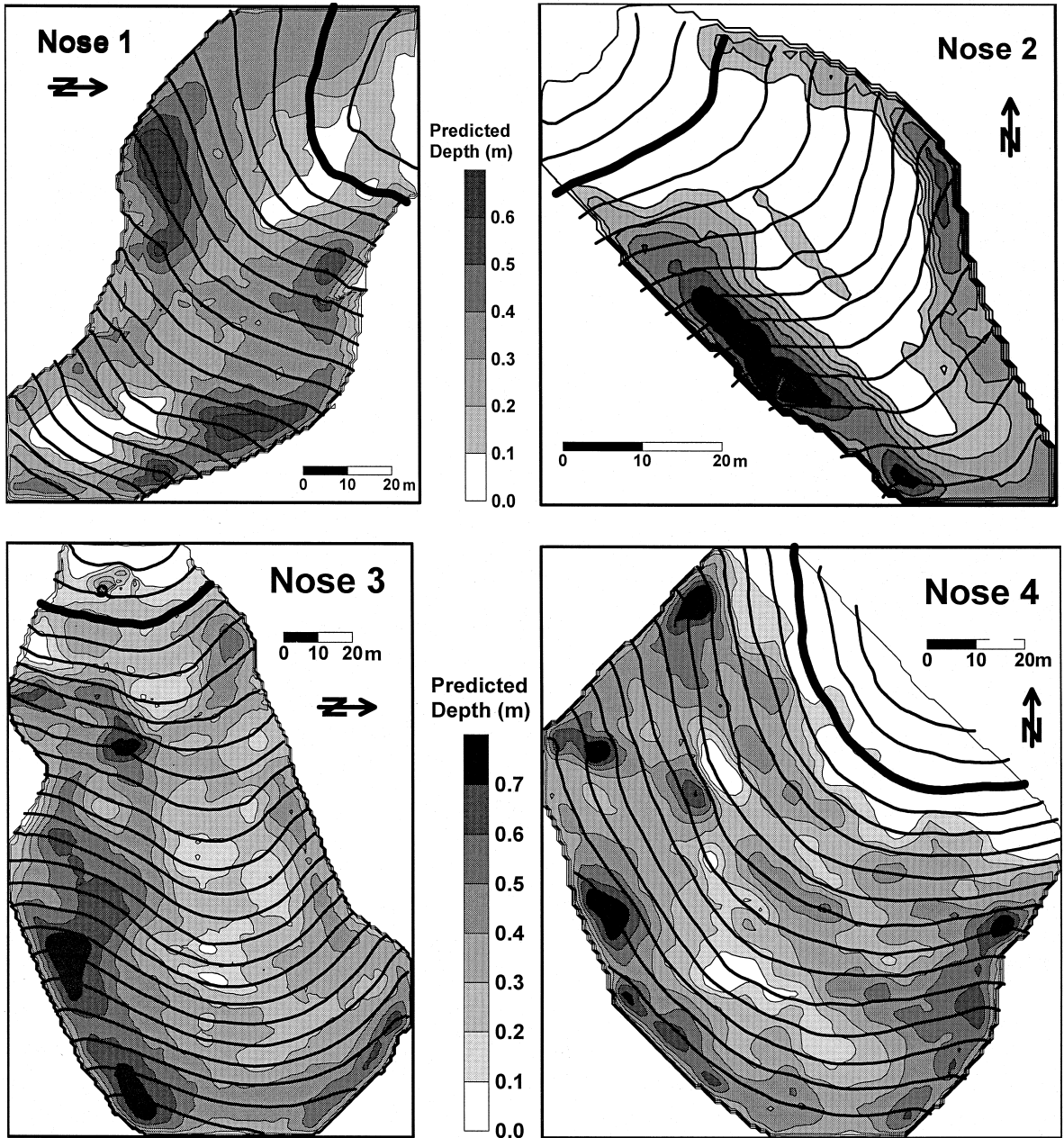


Fig. 9. Predicted depths of soil, in m, after 6000 years of running the soil model with 10-year time steps on all four surveyed noses. These predicted depths are determined using the exponential fit to the data here, shown in Fig. 7, as the function of soil production. Boundary conditions are explained in the text and initial soil thickness is zero. Topographic contour lines are drawn at 2 m, and are the same as Fig. 5. The thickened contour line near the top of each nose shows the cut-off elevation above which we treated predicted depths as upper-boundary artifacts and did not compare them to our observed depths in the area.

separate experiment, when we used an initial thickness of soil of 30 cm, the predicted depths were consistently higher than the observed depths. When we ran the model with this initial condition, the thickness of the soils increased at a rate of about 1 cm every thousand years. However, when we ran the model with zero initial thickness then the thickness of soil sharply increased initially and tended to stabilize into a much more gradual, almost negligible increase after six thousand years. We chose the thickness of soil predicted after 6000 years (starting from zero initial depth) to represent the steady-state condition that we assume in our conceptual framework. We do not suggest, however, that the sites were bare bedrock 6000 ago.

The difference in results between the two initial conditions of soil thickness is due to the interplay of erosion, smoothing of the topography, and rates of soil production. Because the nose axes are more divergent, sediment is transported away from the axes relatively rapidly. Thickness of soil on the axes remains thinner than the surrounding areas and, therefore, the rate of soil production is higher. Over time, the result is that the nose flattens and the model wears down the convexity of the noses. When the initial thickness of soil is 30 cm or greater, the model smoothens the convexity of the noses before the soils could thin enough to reach the thickness of soil on the nose axes observed in the field.

We compared the depths of soil predicted by the model plotted against the measured depths against the ideal, 1:1 relationship (Fig. 10). We show no comparison for nose 2 because inadequate topographic information prevented direct comparison between the predicted depths from the model and our observed depths. Within a factor of about two, the predicted and observed depths correspond on nose 1 and nose 4. Nose 3 shows an underprediction of depth of soil for the deeper soils. Nose 3, however,

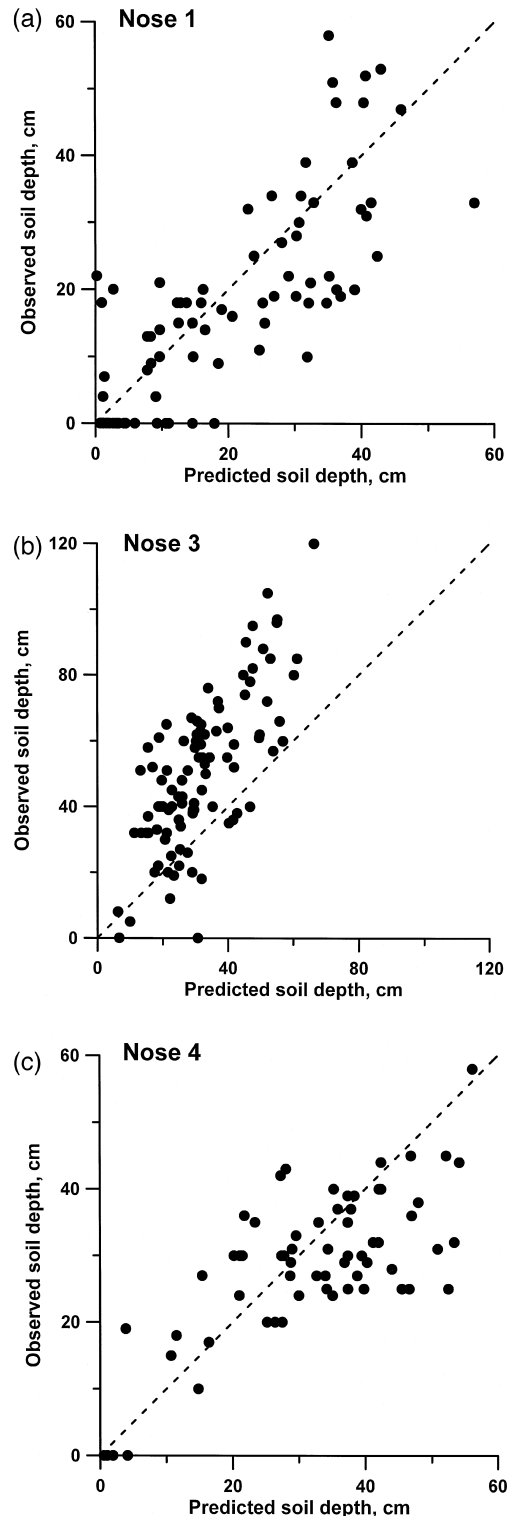


Fig. 10. Observed depth of soil, in cm, vs. predicted for the predicted depths shown by the maps of Fig. 9 and the measured depths from three of the four studied noses: (a) nose 1; (b) nose 3; (c) nose 4. Depth data from nose 2 were too sparse to adequately compare the predicted depths to the observed. Depths were predicted at all points on the noses as contoured in Fig. 9 and are compared at the same points where we measured the depth of the soil.

shows a much larger range of depths over the range of curvature measurements as shown in Fig. 6, and the deeper soils were found in weakly convergent areas. Our conceptual model applies the assumption of a steady state depth of soil only to the divergent areas of the landscape and the deeper soils that we observe may result from, in part, accumulation in locally convergent areas.

## 7. Discussion

### 7.1. Steady-state soil depth

An important assumption that is common to both methods is that the local thickness of soil does not vary with time as soil is produced and transported downhill. This assumption of local steady state is justified at our field sites in several ways. No evidence exists for shallow landsliding or erosion by overland flow on the convex regions that we studied. Soil production, primarily by burrowing mammals, while stochastic, tends not to alter local soil thickness dramatically beyond a few years. Numerical experiments by Dietrich et al. (1995) show that on ridges eroding by diffusive processes, initial arbitrary thickness of soil quickly (in a few thousand years) reaches a local steady-state for a slowly changing curvature. Our modeling results (using much higher resolution topographic data) show that thickness of soil quickly adjusted to local curvature, but because of the boundary conditions and the initial convexity of the nose, curvature slowly changed with time thus causing the local thickness of soil to change. The greater sensitivity to curvature change in our modeling results from the higher resolution topography that we used, which led to larger local variations in elevation and, therefore, curvature. Also, the initial surface used in our model was effectively much rougher and, therefore, smoothed more than the larger scale modeling reported by Dietrich et al. (1995). Because of the rapid thickness of soil adjustment to the initial thickness imposed on the noses observed in our models, we suggest that any adjustment in soil thickness in response to Holocene warming and drying occurred in the early Holocene.

The concentrations of  $^{10}\text{Be}$  and  $^{26}\text{Al}$  provide an independent test for our assumption of steady-state

depth of soil.  $^{10}\text{Be}$  has a half-life roughly twice as long as  $^{26}\text{Al}$  and the ratio of  $^{26}\text{Al}/^{10}\text{Be}$  can be used to help infer the history of erosion and exposure for the samples (Nishiizumi et al., 1993; Nishiizumi et al., 1991). Nishiizumi et al. (1991) illustrate how this measured ratio can be used for such conclusions. The short exposure ages of our samples, resulting from relatively high rates of erosion, means that all our samples should have a  $^{26}\text{Al}/^{10}\text{Be}$  value of about six (Table 1).

A few of our samples show some discrepancy between the measured  $^{26}\text{Al}/^{10}\text{Be}$  ratios and the expected value of 6.0 (Nishiizumi et al., 1991). We were concerned that the difference in the measured  $^{26}\text{Al}/^{10}\text{Be}$  would significantly affect the nuclide-determined function of soil production. When we plot the function of soil production (in the same manner as Fig. 7) using only the concentrations of  $^{10}\text{Be}$  or  $^{26}\text{Al}$  to calculate the rates of soil production we find the following best-fit lines regressed by standard error-weighted least squares (Bevington, 1969): (1) using  $^{10}\text{Be}$  only: soil production =  $(74 \pm 5) \times e^{(-0.022 \pm 0.002 * \text{depth})}$ , (2) using  $^{26}\text{Al}$  only: soil production =  $(79 \pm 7) \times e^{(-0.024 \pm 0.002 * \text{depth})}$ , and (3) using  $^{26}\text{Al}$  and  $^{10}\text{Be}$ : soil production =  $(77 \pm 9) \times e^{(-0.023 \pm 0.002 * \text{depth})}$  (the fit shown in Figs. 7, 8 and 11).

These functions of soil production are statistically the same.

We chose to use the average measurements of  $^{10}\text{Be}$  and  $^{26}\text{Al}$  in our calculation of the function of soil production because we see no independent reason to reject either the  $^{26}\text{Al}$  or the  $^{10}\text{Be}$  data. Three samples differ unequivocally from 6, notable the samples from large bedrock outcrops, TV-4 and TV-5, and the shallow soil mantled, TV-3. Only TV-3 is used in the regression that defines the function of soil production, but its influence on the slope of the line is small because of its larger variance. Samples TV-4 and TV-5 require further discussion. These low  $^{26}\text{Al}/^{10}\text{Be}$  ratios could only arise if, (1) some systematic error occurred in sample analysis (i.e., overestimation of the concentration of  $^{10}\text{Be}$  from incomplete removal of garden variety  $^{10}\text{Be}$ , or underestimation of  $^{26}\text{Al}$  from incomplete dissolution of the sample or errors in AA measurement of the concentration of stable Al in the sample solution) or 2) some complex burial history occurred

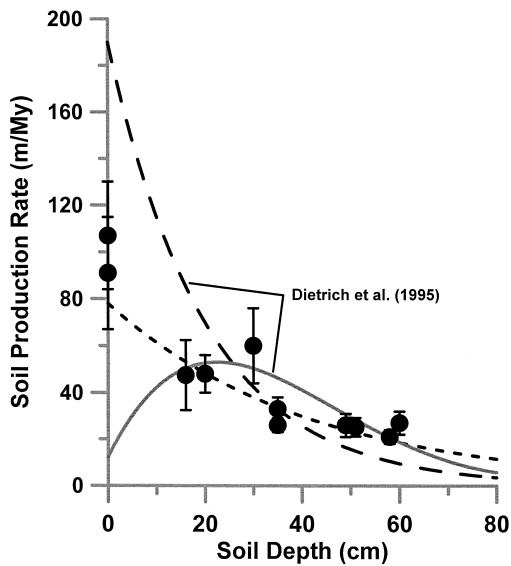


Fig. 11. The exponential best-fit to these data in Fig. 7 plotted with functions of soil production used by Dietrich et al. (1995). We use a linear axis for the rate of soil production here to better illustrate the polynomial function plotted with the solid grey line. The best fit to our data is plotted with the small black dashed line with an intercept of 77 m/My and a slope of  $-0.024$ . The exponential function used by Dietrich et al. (1995) is plotted with a large dashed line, an intercept of 190 m/My, and a slope of  $-0.05$ . The large black dots are the data from Fig. 7 used to derive the exponential best fit for this function of soil production. The convergence of all three curves occurs at about 30 cm of depth in the soil.

during which time the  $^{26}\text{Al}$  decayed faster than the  $^{10}\text{Be}$ . No analytical reason exists to reject the analyses of  $^{10}\text{Be}$  or the  $^{26}\text{Al}$ .

Interestingly, TV-4 and TV-5 are large bedrock outcrops, lithologically different from the other samples, which are physically separated from the other samples by lying at the top of the basin (Fig. 2a inset map and labeled on Fig. 2b). The low ratios could point to some complex geologic history that will require further analysis to be fully understood. Here we choose to interpret these samples with our simple exposure model, and express the difference between the results of  $^{10}\text{Be}$  and  $^{26}\text{Al}$  with the large uncertainty in the estimates of erosion for these samples. The only conclusion that we draw from these samples, and TV-2, is that large bedrock outcrops are eroding, or lowering, at significantly slower rates than the soil-mantled part of the landscape. The

uncertainty between the  $^{10}\text{Be}$  and the  $^{26}\text{Al}$  based results does not alter this conclusion.

## 7.2. Soil depth and curvature

The curvature–depth analysis depends on using an appropriate spatial scale to calculate curvature and on correctly identifying the soil–bedrock boundary. Several reasons exist to explain why this analysis may break down. The first is that the identification of the boundary may be incorrect because large pieces of rock in the colluvium are very similar to the fractured bedrock. We found that a soil auger often could not get past colluvial stones and would, therefore, not reach the soil–bedrock boundary. The presence of stone-lines would have further complicated our measurements. In addition to relying on soil pits for our measurements we extended the pits beyond the soil–bedrock boundary to insure that the observed fractured bedrock was not a stone-line. Even if the actual identification of the soil–bedrock boundary was correct, the observed depth of soil may not reflect the long-term average depth. If the dominant process of soil production-transport had changed recently because of land-use or climate changes, then the depth of soil may be still adjusting toward a local steady state in response to the new processes. For example, if the mid-Holocene climate in this area was significantly drier (Rypins et al., 1989) then rates of soil production from biotic activity may have slowed in comparison to the rates in wetter conditions. The current depth–curvature relationship could still be adjusting from such a mid-Holocene condition. Numerical modeling, however, indicates relatively rapid adjustment of the local depth of soil, and suggests that this probably is not the case.

Fernandes and Dietrich (1997) solve a diffusion-type equation in one-dimension (1-D equivalent to our Eq. (4) written for the change in elevation of the ground surface rather than the soil–bedrock interface) with parameters specific to this field area here to explore the equilibrium condition of convex hill-tops. Their analysis of morphologic relaxation time for hillslope profiles after just a twofold change in either diffusivity or the rate of base-level downcutting suggests that the time to morphologic equilibrium is on the order of seventy thousand years or

more a for hillslope length of 25 m. The modeling we report here and that reported by Dietrich et al. (1995) indicates that thickness of soil approaches a local steady state in less than ten thousand years. Hillslopes can, therefore, undergo slow, progressive morphologic evolution while remaining mantled by soil with local depths that are approximately constant over thousands of years. Thus, a systematic relationship between curvature and the local depth of soil as we observe here (Fig. 6), can express landscape disequilibrium while adhering to the assumption of a local steady-state depth.

In their modeling of the thickness of soil, Dietrich et al. (1995) used functions of soil production estimated from two field-based observations of soil production. They used net erosion recorded in thickened valley deposits to set the rate of soil production under 30 cm of soil, the average depth for the side slopes contributing to the valley axis. They also suggested, based on field observations, that soil production approached zero under soil depths greater than 1 m. Fig. 11 shows a remarkable intersection of these functions of soil production with the one reported here around a soil depth of 30 cm. Their exponential function has an intercept of 190 m/My, compared to 77 m/My reported here, and a slope of  $-0.05$  compared to  $-0.024$ . Whereas this agreement is encouraging, and helps support the spatial variation in the thickness of soil that they predicted, the predicted depths of soil on the noses here using the exponential function of Dietrich et al. (1995) do not agree as well with observed. Using their function results in significant overprediction of the depth soil on nose 1 and nose 4, whereas nose 3 retains a similar relationship to Fig. 10c (Fig. 12). These differences can be explained by the higher rate of soil production estimated by the exponential fit intercept of Dietrich et al. (1995) and the steeper slope of their function. The steeper slope of their estimated function means that bedrock under thicker soils produces soil more slowly than we found in our study and explains the gentler trend in the predicted versus observed depths.

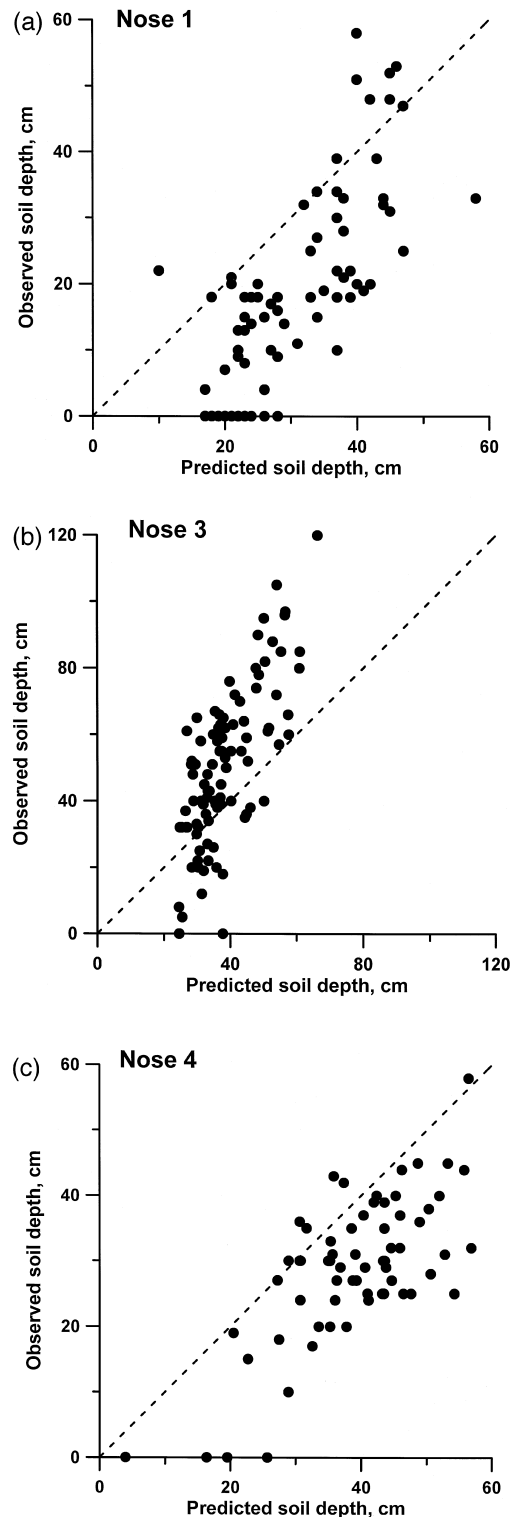


Fig. 12. Observed versus predicted soil depths for (a) nose 1; (b) nose 3; (c) nose 4 plotted in the same manner as Fig. 10, but using the exponential function of Dietrich et al. (1995) shown in Fig. 11.

The exponential function of soil production shows the highest rate of soil production occurring under no soil cover. If burrowing gophers and the penetration of roots from vegetation are the primary agents of mechanical disruption of the bedrock, then it may be that some limited soil mantle is necessary for the highest rate of soil production. On the other hand, the bedrock that emerges at the ground surface is typically highly fractured and friable, and probably undergoes accelerated breakdown as a consequence of wetting and drying. Periodic fires may also contribute to the rapid breakdown of exposed rock. Without further investigation into the mechanisms of soil production we cannot reject the possibility of a 'humped' function of soil production, but the evidence reported here strongly supports a simple exponential function.

### 7.3. *Landscape equilibrium*

A variety of observations, in addition to the depth–curvature relationship, suggest that this study site is not in morphologic equilibrium. Large bedrock outcrops are eroding at rates significantly lower than the rest of the landscape. The largest outcrop analyzed, TV-4, sticks up above the surrounding soil by an average of about 10 m. This difference in elevation would develop over about 270 000 years if TV-4, which is eroding at about 40 m/My, emerged from a surrounding landscape lowering at the maximum rate of 77 m/My. This is a long term, local perturbation of the topography. Furthermore, the  $^{10}\text{Be}/^{26}\text{Al}$  ratio of this and other large outcrops suggests that a complex history of burial and exposure occurred here. Smaller outcrops are scattered across the hillslopes and can cause local topographic perturbations that may persist for millennia after the outcrop is stripped away by erosion.

The average rates erosion from the two subcatchments in the steeper areas of the headwaters (Fig. 2a inset and b) are higher than the rates of soil production on the noses in the gentler slopes of the lower part of the study basin. The only nose in the steeper part of the catchment that we surveyed (Nose 2, shown by the X in Fig. 2a inset and labeled on 2b) had distinctly thinner soils and lacked the areas of low curvature (and, therefore, a low rate of soil production) found on other noses. Additionally, most

of the shallow landslides mapped in this study area occurred in the steeper part of the basin (Dietrich et al., 1993). These observations together suggest that the lower, more gently sloping parts of the study area are eroding distinctly more slowly than the steeper headwaters region. More speculatively, but consistent with these observations, the surrounding ridge of the catchment is sloping relatively gently. We suggest that a wave of incision moved up the catchment, with the lower region in a state of 'relaxation' (e.g., Ahnert, 1987), or slowing rate of erosion.

The tectonic setting of this study site is complex. To the east and west major active strike-slip fault systems exist. Although this site is east of the San Andreas Fault, it is part of a transpressional zone, components of which are advecting northwards (e.g., Aydin and Page, 1984; Prescott and Yu, 1986; Page, 1992). San Francisco Bay (4 km south of the site) is subsiding at 0.07–0.8 mm/year (e.g., Atwater et al., 1977; Prims and Furlong, 1995) whereas Quaternary marine terraces rise progressively higher north of the site (e.g., Wehmiller et al., 1977). Given this setting, it is extremely unlikely that tectonic-induced river incision has been constant over the time scale necessary for morphologic equilibrium of the landscape to develop.

Climatic variations in the Quaternary have also contributed to the disequilibrium here. A Holocene alluvial and colluvial fill occurs in the main valley floor of the study site as well as in most of the valley network (Montgomery and Dietrich, 1989; Dietrich et al., 1993). The lowering of sea level induced by glaciation may have caused periodic channel incision by lowering the base-level (the Pacific Ocean is currently less than 2 km west of the study site). Higher rates of rainfall and runoff during the Pleistocene also may have led to periods of active channel incision. If these periods of increased channel incision did occur, then the base of the hillslopes were subjected to periodic steepening that would have then advanced upslope, leading to long periods of morphologic adjustment.

The curvature variation that we observe suggests disequilibrium in the morphology of the landscape and it leads to the spatial variation in soil thickness. Curvature variation is not randomly distributed. The axes of all four surveyed noses are systematically the most strongly curved part of the noses. This curva-

ture is nearly all plan curvature rather than profile curvature. It is possible that this spatial variation of curvature is an expression of nonlinear processes of diffusion sediment transport (Roering et al., 1997, in press). Even so, the spatial variation of soil thickness associated with the curvature would still imply non-uniform rates of soil production. Given the modest gradients of these study sites, we believe that an approximation of linear diffusion is applicable and that systematic flattening away from the nose axes may have resulted from a reduced rate of incision in adjacent valleys. We are exploring the possibility of nonlinear sediment transport through further modeling and field work.

## 8. Conclusion

We suggest a conceptual framework for predicting soil thickness on a real landscape using a process-based model. This study supports the framework of Dietrich et al. (1995) and uses our (Heimsath et al., 1997) field-derived function of soil production. Our quantitative determination of the function of soil production has enabled reasonably accurate prediction of spatial variations in soil thickness on fine-scale topographic noses. We find, however, that predicting soil thickness depends on the boundary and initial conditions, the grid size, the model run time, as well as the function of soil production. The modeling results presented here to predict the thickness of soil help verify a method that could be applied at other sites to help understand the impacts of lithology, climate, and tectonics on landscape evolution. Additionally, such methods could be applied to evaluate potential impacts of land-use in regions where soil thickness may be sensitive to changes in the dominant geomorphic processes by identifying how soil thickness could change when, for example, the diffusivity changes with changing strategies of land-use.

The variable thickness of soil that we observe is a function of topographic curvature and suggests an inverse relationship between soil production and depth of soil. This relationship, along with several other observations about rates of erosion and landscape form, suggest that the landscape is not in morphologic equilibrium. This disequilibrium is not

surprising given the complex tectonic setting of the study area and the likely residual influence of an oscillating climate on a landscape undergoing relatively modest rates of erosion. We do not, however, know the exact cause of the systematic variation in curvature observed here.

Extension of these methods to new field sites will require very high-resolution topographic surveys and will benefit from higher spatial resolution of depth measurement than we used here. More densely spaced measurements of soil depth will enable accurate depiction of the bedrock surface, which can then be tested as an initial condition in modeling the development of the soil mantle. The topographic surveys should also include the complete topography, from ridge tops to valley bottoms, which can then be used to help clearly define the boundary conditions. Further application of the nuclide method would benefit from quartz-rich underlying bedrock and both methods depend on being able to clearly identify the soil–bedrock interface. On landscapes undergoing very high rates of erosion, the nuclide method may become impractical if the concentrations of the nuclides are below measurable levels. It may also be that landscapes, where the linear diffusive sediment transport law is applicable, may be limited and instead other processes of mass wasting, such as landsliding, may predominate. Despite such potential limitations, this approach has empirically quantified the function of soil production for the first time and should be broadly applicable to other landscapes.

## Acknowledgements

We thank K. Heimsath and L. Cossey for field and lab assistance, D. DePaolo for laboratory space, D. Lal for suggestions and the Golden Gate National Recreation Area for access to our study site. D. Bellugi adapted the numerical model to conditions here and conducted the modeling efforts. This work was partially performed under the auspices of the US DOE by Lawrence Livermore National Laboratory under contract W-7405-Eng-48 and was supported by Cal Space, IGPP-LLNL GS96-05, NSF EAR-9527006, with NASA Global Change and Switzer Environmental fellowships to AMH. We thank Gregory Hancock and an anonymous reviewer for their helpful suggestions.

## References

- Ahnert, F., 1967. The role of the equilibrium concept in the interpretation of landforms of fluvial erosion and deposition. In: Macar, P. (Ed.), *L'évolution des versants*. University of Liege, Liege, pp. 23–41.
- Ahnert, F., 1987. Approaches to dynamic equilibrium in theoretical simulations of slope development. *Earth Surface Processes and Landforms* 12, 3–15.
- Anderson, R.S., Humphrey, N.F., 1989. Interaction of weathering and transport processes in the evolution of arid landscapes. *Quantitative Dynamic Stratigraphy*, 349–361.
- Armstrong, A.C., 1987. Slopes, boundary conditions, and the development of convex–concave forms—some numerical experiments. *Earth Surface Processes and Landforms* 12, 17–30.
- Arnett, R.R., 1971. Slope form and geomorphological process: an Australian example. *Institute of British Geographers, Special Publication* 3, 81–92.
- Atwater, B.F., Hedel, C.W., Helley, E.J., 1977. Late Quaternary depositional history, Holocene sea-level changes, and vertical crustal movement, southern San Francisco Bay, California. *U.S. Geological Survey Professional Paper* 1014, 15.
- Aydin, A., Page, B., 1984. Diverse Pliocene–Quaternary tectonics in a transform environment, San Francisco Bay region, California. *GSA Bulletin* 95 (11), 1303–1377.
- Bevington, P.R., 1969. *Data Reduction and Error Analysis for the Physical Sciences*. McGraw-Hill, New York.
- Bierman, P.R., 1994. Using in situ produced cosmogenic isotopes to estimate rates of landscape evolution; a review from the geomorphic perspective. *Journal of Geophysical Research, B, Solid Earth and Planets* 99 (7), 13885–13896.
- Bierman, P., Steig, E.J., 1996. Estimating rates of denudation using cosmogenic isotope abundances in sediment. *Earth Surface Processes and Landforms* 21, 125–139.
- Black, T.A., Montgomery, D.R., 1991. Sediment transport by burrowing animals, Marin county, California. *Earth Surface Processes and Landforms* 16, 163–172.
- Carson, M.A., Kirkby, M.J., 1972. *Hillslope form and process*. Cambridge University Press, New York, 475 pp.
- Cerling, T.E., Craig, H., 1994. Geomorphology and in-situ cosmogenic isotopes. *Annual Reviews Earth Planetary Sciences* 22, 273–317.
- Cox, N.J., 1980. On the relationship between bedrock lowering and regolith thickness. *Earth Surface Processes and Landforms* 5, 271–274.
- Cressie, N.A.C., 1991. *Statistics for Spatial Data*. Wiley, New York, 900 pp.
- Culling, W.E.H., 1963. Soil creep and the development of hillslope slopes. *Journal of Geology* 71 (2), 127–161.
- Davis, J.C., Proctor, I.D., Southon, J.R., Caffee, M.W., Heikkinen, D.W., Roberts, M.L., Moore, T.L., Turteltaub, K.W., Nelson, D.E., Loyd, D.H., Vogel, J.S., 1990. LLNL/UC AMS facility and research program. *Nuclear Instruments Methods in Physics Research, Section B (B52)*, 269–272.
- Davis, W.M., 1892. The convex profile of badland divides. *Science* 20, 245.
- DeRose, R.C., Trustrum, N.A., Blaschke, P.M., 1991. Geomorphic change implied by regolith-slope relationships on steep-land hillslopes, Taranaki, New Zealand. *Catena* 18, 489–514.
- Dietrich, W.E., Wilson, C.J., Montgomery, D.R., McKean, J., Bauer, R., 1992. Erosion thresholds and land surface morphology. *Geology (Boulder)* 20 (8), 675–679.
- Dietrich, W.E., Wilson, C.J., Montgomery, D.R., McKean, J., 1993. Analysis of erosion thresholds, channel networks, and landscape morphology using a digital terrain model. *Journal of Geology* 101 (2), 259–278.
- Dietrich, W.E., Reiss, R., Hsu, M.-L., Montgomery, D.R., 1995. A process-based model for colluvial soil depth and shallow landsliding using digital elevation data. *Hydrological Processes* 9, 383–400.
- Ellis, M., Merritts, D. (Eds.), 1994. *Special section on Tectonics and Topography. Journal of Geophysical Research—Solid Earth*, 99. American Geophysical Union, pp. 12135–20321.
- Fernandes, N.F., Dietrich, W.E., 1997. Hillslope evolution by diffusive processes: the time scale for equilibrium adjustments. *Water Resources Research* 33 (6), 1307–1318.
- Gessler, P.E., Moore, I.D., McKenzie, N.J., Ryan, P.J., 1995. Soil-landscape modeling and spatial prediction of soil attributes. *Int. J. Geographical Information Systems* 9 (4), 421–432.
- Gilbert, G.K., 1877. *Report on the Geology of the Henry Mountains (Utah)*, United States Geological Survey, Washington, DC.
- Gilbert, G.K., 1909. The convexity of hilltops. *Journal of Geology* 17 (4), 344–350.
- Granger, D.E., Kirchner, J.W., Finkel, R., 1996. Spatially averaged long-term erosion rates measured from in situ-produced cosmogenic nuclides in alluvial sediment. *J. Geol.* 104 (3), 249–257.
- Hack, J.T., 1960. The interpretation of erosional topography in humid temperate regions. *Am. J. Sci.* 258A, 80–97.
- Heimsath, A.M., Dietrich, W.E., Nishiizumi, K., Finkel, R.C., 1997. The soil production function and landscape equilibrium. *Nature* 388, 358–361.
- Howard, A.D., 1994. A detachment-limited model of drainage basin evolution. *Water Resources Research* 30 (7), 2261–2285.
- Howard, A.D., 1997. Badland morphology and evolution: interpretation using a simulation model. *Earth Surface Processes and Landforms* 22, 211–227.
- Johnson, D.L., 1990. Biomantle evolution and the redistribution of earth materials and artifacts. *Soil Science* 149 (2), 84–102.
- Kirkby, M.J., 1971. Hillslope process–response models based on the continuity equation. *Institute of British Geographers Special Publication* 3, 15–30.
- Kohl, C.P., Nishiizumi, K., 1992. Chemical isolation of quartz for measurement of in-situ-produced cosmogenic nuclides. *Geochim. Cosmochim. Acta* 56, 3583–3587.
- Kooi, H., Beaumont, C., 1994. Escarpment evolution on high-elevation rifted margins: insights derived from a surface processes model that combines diffusion, advection, and reaction. *J. Geophys. Res.* 99 (B6), 12191–12209.
- Koons, P.O., 1989. The topographic evolution of collisional mountain belts; a numerical look at the Southern Alps, New Zealand. *Am. J. Sci.* 289 (9), 1041–1069.

- Lal, D., 1958. Investigations of nuclear interactions produced by cosmic rays. PhD Thesis, Tata Institute of Fundamental Research, Bombay, India.
- Lal, D., 1988. In situ-produced cosmogenic isotopes in terrestrial rocks. *Annu. Rev. Earth Planet. Sci.* 16, 35–388.
- Lal, D., 1991. Cosmic ray labeling of erosion surfaces: in situ nuclide production rates and erosion models. *Earth and Planetary Science Letters* 104, 424–439.
- Lal, D., Arnold, J.R., 1985. Tracing quartz through the environment. *Proc. Indian Acad. Sci. (Earth Planet. Sci.)* 94 (1), 1–5.
- Lutz, H.J., 1960. Movement of rocks by uprooting of forest trees. *Am. J. Sci.* 258, 752–756.
- McKean, J.A., Dietrich, W.E., Finkel, R.C., Southon, J.R., Caffee, M.W., 1993. Quantification of soil production and downslope creep rates from cosmogenic  $^{10}\text{Be}$  accumulations on a hillslope profile. *Geology (Boulder)* 21 (4), 343–346.
- Montgomery, D.R., Dietrich, W.E., 1988. Where do channels begin?. *Nature* 336 (6196), 232–234.
- Montgomery, D.R., Dietrich, W.E., 1989. Source areas, drainage density, and channel initiation. *Water Resources Research* 25 (8), 1907–1918.
- Montgomery, D.R., Dietrich, W.E., 1995. Hydrologic processes in a low-gradient source area. *Water Resources Research* 31 (1), 1–10.
- Moore, I.D., Grayson, R.B., Ladson, A.R., 1991. Digital terrain modeling: a review of hydrological, geomorphological, and biological applications. *Hydrological Processes* 5, 3–30.
- Moore, I.D., Gessler, P.E., Nielsen, G.A., Peterson, G.A., 1993a. Soil attribute prediction using terrain analysis. *Soil Science Society of America Journal* 57, 443–452.
- Moore, I.D., Lewis, A., Gallant, J.C., 1993b. Terrain attributes; estimation methods and scale effects. In: Jakeman, A.J. et al. (Eds.) *Modeling Change in Environmental Sciences*. Wiley, New York.
- Nishiizumi, K., Lal, D., Klein, J., Middleton, R., Arnold, J.R., 1986. Production of  $^{10}\text{Be}$  and  $^{26}\text{Al}$  by cosmic rays in terrestrial quartz in situ and implications for erosion rates. *Nature (London)* 319 (6049), 134–136.
- Nishiizumi, K., Winterer, E.L., Kohl, C.P., Klein, J., Middleton, R., Lal, D., Arnold, J.R., 1989. Cosmic ray production rates of  $^{10}\text{Be}$  and  $^{26}\text{Al}$  in quartz from glacially polished rocks. *J. Geophys. Res.* 94 (B12), 17907–17915.
- Nishiizumi, K., Kohl, C.P., Arnold, J.R., Klein, J., Fink, D., Middleton, R., 1991. Cosmic ray produced  $^{10}\text{Be}$  and  $^{26}\text{Al}$  in Antarctic rocks: exposure and erosion history. *Earth Planetary Sci. Lett.* 104, 440–454.
- Nishiizumi, K., Kohl, C.P., Arnold, J.R., Dorn, R., Klein, J., Fink, D., Middleton, R., Lal, D., 1993. Role of in situ cosmogenic nuclides  $^{10}\text{Be}$  and  $^{26}\text{Al}$  in the study of diverse geomorphic processes. *Earth Surface Processes and Landforms* 18, 407–425.
- Page, B., 1992. Tectonic setting of the San Francisco Bay region. Special publication. California Division of Mines and Geology 62, 53.
- Prescott, W.H., Yu, Y., 1986. Geodetic measurement of horizontal deformation in the northern San Francisco Bay region, California. *J. Geophys. Res.* 91 (7), 7475–7484.
- Prims, J., Furlong, K.P., 1995. Subsidence of San Francisco Bay; blame it on Salinia. *Geology* 23 (6), 559–562.
- Rantz, S.E., 1968. Average annual precipitation and runoff in north coastal California. US Geological Survey Hydrological Atlas 298, scale 1:1,000,000.
- Reneau, S.L., Dietrich, W.E., Dorn, R.I., Berger, C.R., Rubin, M., 1986. Geomorphic and paleoclimatic implications of latest Pleistocene radiocarbon dates from colluvium-mantled hollows, California. *Geology* 14 (8), 655–658.
- Reneau, S.L., 1988. Depositional and erosional history of hollows: application to landslide location and frequency, long-term erosion rates, and the effects of climatic change. PhD Thesis, University of California, Berkeley, CA, 328 pp.
- Reneau, S.L., Dietrich, W.E., Donahue, D.J., Jull, T.A., Rubin, M., 1990. Late Quaternary history of colluvial deposition and erosion in hollows, Central California Coast Ranges. *GSA Bulletin* 102 (7), 969–982.
- Reneau, S.L., Dietrich, W.E., 1991. Erosion rates in the southern Oregon coast range: evidence for an equilibrium between hillslope erosion and sediment yield. *Earth Surface Processes and Landforms* 16 (4), 307–322.
- Roering, J.J., Kirchner, J.W., Dietrich, W.E., 1997. Evidence for a non-linear diffusive mass wasting transport law and implications for hillslope evolution in the Oregon Coast Range. *EOS, Proc. of the AGU Fall meeting*, p. 212.
- Roering, J.J., Kirchner, J.W., Dietrich, W.E., in press. Evidence for non-linear, diffusive sediment transport on hillslopes and implications for landscape evolution. *Water Resources Research*.
- Rosenbloom, N.A., Anderson, R.S., 1994. Hillslope and channel evolution in a marine terraced landscape, Santa Cruz, California. *J. Geophys. Res.* 99 (B7), 14013–14029.
- Rypins, S., Reneau, S.L., Byrne, R., Montgomery, D.R., 1989. Palynologic and geomorphic evidence for environmental change during the Pleistocene–Holocene transition at Point Reyes peninsula, central coastal California. *Quaternary Research (New York)* 32 (1), 72–87.
- Tucker, G.E., Slingerland, R.L., 1994. Erosional dynamics, flexural isostasy, and long-lived escarpments—a numerical modeling study. *J. Geophys. Res., Solid Earth* 99 (B6), 12229–12243.
- Wahrhaftig, C., 1984. Structure of the Marin headlands block, California: a progress report. *Franciscan Geology of Northern California* 43, 31–50.
- Wehmiller, J.F., Lajoie, K.R., Kvenvolden, K.A., Peterson, E., Belknap, D.F., Kennedy, G.L., Addicott, W.O., Vedder, J.G., Wright, R.W., 1977. Correlation and chronology of Pacific Coast marine terrace deposits of continental United States by fossil amino acid stereochemistry; technique, evaluation, relative ages, kinetic model ages, and geologic implications. USGS, 191 pp.
- Young, A., 1963. Some field observations of slope form and regolith, and their relation to slope development. *Transactions of the Institute of British Geographers* 32, 1–29.